Geospatial Assessment of Mangrove Dynamics in Relation to Climate Variability

Abdi-Basid ADAN, 2024

E-mail addresses: abdi-basid@outlook.com

Abstract

Understanding changes in mangrove ecosystems driven by human activities, climate change, and environmental variations is essential for effective ecological management. The study analyze the spatiotemporal variability of the Normalized Difference Vegetation Index (NDVI) and their responses to parameters such as sea level (SL), Potential Evapotranspiration (PET), rainfall (RF), Standardized Precipitation Index (SPI-1 month), soil moisture (SM), minimum temperature (TN), and maximum temperature (TX) within the study area. Trends, relative influences, spatial autocorrelation, and relationships between NDVI and climatic-environmental variables, as well as partial correlations, were analyzed using the Mann-Kendall monotonic trend test (MKMT), Relative Weight Analysis (RWA), partial correlation coefficients (PCC), and Multiple Linear Regression (MLR) methods. The spatiotemporal patterns of NDVI, EVI, and SAVI display similar dynamics, showing a reduction in bare soil and an increase in sparse and dense vegetation from 1987 to 2022. Nevertheless, zones of degradation were observed, particularly in southern in 2022 compared to 1987, as indicated by NDVI, EVI, and SAVI. These zones coincide with areas of increased salinity concentration according to the VSSI index over the same period. A notable deterioration in NDVI (> 0.2) was recorded from 2000 to 2012. The interannual trend of NDVI is slightly declining. Additionally, analyses with Mann-Kendall and Theil-Sen slope reveal that TN, TX, PET, and SPI-1 show increasing trends, though not statistically significant, while SM and LST show decreasing trends. For environmental variables, SL indicates an upward trend. Further, partial correlation analysis identifies SL, TN, SPI-1, TX, and PET as the primary climatic factors controlling vegetation dynamics during the JJAS season, with PCC values of -0.89, 0.87, 0.77, -0.76, -0.75, and 0.86 with NDVI, respectively. These findings underscore the significant influence of select environmental factors on the spatiotemporal dynamics of mangrove vegetation, providing insights critical for conservation and management efforts.

Key words: Mangrove, spatiotemporal analysis, Climate change, environmental variability Remote sensing,

Climatological and Environmental Datasets

To investigate climate change and its impact on vegetation, several datasets were used in combination, including MODIS Terra LST data, potential evapotranspiration, GLDAS soil moisture, CHIRPS V2 precipitation, minimum and maximum air temperatures from ERA5, JTWC cyclone tracks, as well as sea level data from SHOM. These were combined with Landsat 4-7 and SPOT 3-4 satellite bands, which were employed to calculate the NDVI, EVI, SAVI, and SSVI indices (Table 1 and Tables S1 and S2, Supplementary Material). The CHIRPS precipitation dataset is an essential resource that delivers a high-quality and long-term record of precipitation by combining satellite and in-situ data (Funk et al., 2015). Moreover, for surface air temperature, the ERA5 dataset offers a comprehensive collection of atmospheric variables, significantly enhancing accuracy and reliability, which is crucial for climate research and monitoring (Hersbach et al., 2020). The data provided by The Joint Typhoon Warning Center (JTWC) is vital for tracking cyclone paths, enabling effective disaster preparedness and response efforts. Indeed, the analysis of cyclone track data enables us to determine whether a cyclone has traversed these three sites during the period from 1987 to 2022, and to assess whether this coincides with periods of degradation, a finding that is also supported by Camberlin et al. (2024). Remote sensing data, particularly from Landsat, which has been operational since 1972, provides a consistent and reliable source of Earth observation data, with a 16-day revisit period and 30 m spatial resolution for surface reflectance (Table S1). This high temporal and spatial resolution make Landsat ideal for long-term monitoring of land cover changes (Fen et al., 2006). Additionally, Landsat 7 is one of the best products for monitoring mangroves, utilizing the combination of bands 3 (0.63-0.69 μ m), 4 (0.77–0.90 μ m), 5 (1.55–1.75 μ m), and 7 (2.09–2.35 μ m) (Li et al., 2019). Moreover, SPOT satellites, operational since 1986, provide high-resolution Earth observation data with spatial resolutions of 10 m and 20 m across three spectral bands: green (0.5 - 0.59 µm), red (0.61 - 0.68 μm), and near infrared (0.79 - 0.89 μm) (Table S2). This spectral configuration enhances sensitivity to chlorophyll, thereby facilitating the assessment of vegetation health. Furthermore, the SPOT system ensures complete Earth coverage within a 26-day cycle, positioning it as a crucial tool for monitoring environmental changes. The SPOT 3 and SPOT 4 satellites not only maintain continuity of services but also enhance capabilities by incorporating the latest advancements in French space technology (Courtois et al., 1986). On the other hand, the GLDAS product for soil moisture offers crucial insights into terrestrial hydrology. This dataset enables researchers to analyze soil moisture dynamics and understand their influence on weather and climate patterns (Bi et al., 2016). MODIS Land Surface Temperature (LST) data play a significant role in elucidating the interactions between land surface processes and climate variability, serving various applications within environmental science (Reiners et al., 2023).

Table 1. Characteristics of Climate and Oceanographic Data Sources.

Source	Variable	Temporal	Spatial	References	
		availability	resolution		
Climate Hazards Center, University of				Funk et al., 2015	
California, Santa Barbara	Precipitation/SPI	1981 - présent	0.05°		
NASA, Moderate Resolution Imaging	Land Surface			Reiners et., 2023	
Spectroradiometer (MODIS)	Temperature	2000 - présent	1 km		
U.S. Geological Survey (USGS)	Vegetation index based	1984 - présent	30 m	Li et al., 2019	
	on LandSat				
Centre National d'Études Spatiales	Vegetation index based			Courtois et al., 1986	
(CNES)	on SPOT	1986 - Présent	10 - 20 m		
NASA MODIS Land Science Team	Potential	2000 - Présent	1 km	Mu et al., 2011	
	Evapotranspiration				
NASA Goddard Earth Sciences Data				Bi et al., 2016	
and Information Services	Soil Moisture	2000 - présent	0.25°		
		_			
European Centre for Medium-Range	Maximum and			Hersbach et al., 2020	
Weather Forecasts (ECMWF)	Minimum air	1959 - présent	0.25°		
	Temperature				
Joint Typhoon Warning Center	Cyclone Tracks	1982 - présent		JTWC, 2022	
(JTWC)					
SHOM	Sea level	1980 - présent		SHOM, 2022	
WorldPop	Buildings	2001–2021	100 m	Dooley et al., 2020	

Anthropogenic variables

To analyze the impact of human activities on vegetation in the region, we used WorldPop data, which offers a spatial resolution of approximately 100 meters (3 arc seconds) and is referenced to the WGS84 coordinate system (Dooley et al., 2020). Grid cells without any building footprints are marked as NAs. This dataset provides building counts within each grid cell, where each building is assigned to the grid cell containing the centroid of its footprint. These building counts serve as proxies for estimating anthropogenic and activity in the area.

Methodology

The satellite images utilized in this study were selected based on a cloud cover threshold of less than 20%, specifically corresponding to the dry and hot season (June to September, JJAS).

Vegetation Index calculation

The Normalized Difference Vegetation Index (NDVI) is commonly used as a reliable estimator of light interception by plant canopies (Hatfield et al., 2010). However, NDVI is sensitive to soil background noise, an issue that the Soil-Adjusted Vegetation Index (SAVI) was developed to

address (Huete et al., 1994). By incorporating soil-adjustment factors, SAVI effectively reduces soil-related interference (Huete et al., 1988). In addition to SAVI, the Enhanced Vegetation Index (EVI) improves upon NDVI by including not only the red and near-infrared (NIR) bands but also a blue band. Furthermore, EVI incorporates soil adjustment factors and atmospheric resistance terms to correct for aerosol influence on the red band, enhancing its performance in areas with high aerosol content (Tsalyuk et al., 2017). For soil salinity estimation, the Vegetation Soil Salinity Index (VSSI) has proven to be a suitable index, offering effective results in detecting and assessing soil salinity levels (Nguyen et al., 2020). The mathematical equations for the indices discussed above are presented in Table 2.

Table 2. Vegetation indices which have been considered in this study.

Spectral Index	Equation	Reference		
Normalized Difference	$NDVI = \frac{(NIR - red)}{(red)^{-1}}$	Nguyen et al.,		
Vegetation Index	$NDVI = \frac{NDVI}{(NIR + red)}$	2020		

2.1.1 Relationship between geospatial indicator and climate variables

2.1.1.1 Theil-Sen slope test and Mann-Kendall significance test

The non-parametric Mann-Kendall Monotonic Trend (MKMT) test is widely recognized as one of the most commonly applied methods for detecting trends in time series data (Chisola et al., 2016). This test is particularly useful for identifying non-linear trends, evaluating both upward and downward monotonic changes over a specified time period (Lamchin et al., 2019). The MKMT test statistic (S) is determined by assessing the number of increasing or decreasing value pairs over time at each pixel (Hussien et al., 2023). This statistic ranges from -1 to +1, where a value of +1 signifies a consistent upward trend without any decline, while a value of -1 represents a continuous downward trend. A value of 0 indicates the absence of a consistent trend. The formula for calculating the MKMT test statistic (S) in time series analysis is outlined by Hussien et al. (2023):

$$S = \sum_{i=1}^{n-1} \sum_{j=i+1}^{n} sign(NDVI_i - NDVI_j)$$
(1)

Where

$$sign(NDVI_i - NDVI_j) = \begin{cases} +1 & ifNDVI_i - NDVI_j < 0 \\ 0 & ifNDVI_i - NDVI_j = 0 \\ -1 & ifNDVI_i - NDVI_j > 0 \end{cases}$$

$$(2)$$

Therefore:

$$\frac{S-1}{\sqrt{var(S)}}, S > 0$$

$$Z = 0, S = 0$$

$$\frac{S+1}{\sqrt{var(S)}}, S < 0$$
(3)

Where n is the number of data points, and $NDVI_i$ and $NDVI_j$ represent the values at time periods i and j (with i > j), sign is the function used to compare the data points from these two periods. When the absolute value of Z exceeds 1.96, the trend in the time series is considered significant at the 0.05 level.

The Theil-Sen slope estimator determines the overall trend in the time series by calculating the slope between each pair of data points and then taking the median of these slopes as the representative trend. The mathematical equation is given by Wand et al. (2020):

$$slope = Median \times \frac{NDVI_i - NDVI_j}{j - i}, \forall j > i$$
(4)

Where slope represents the median of the slopes calculated from all data pairs. If the slope is greater than 0, it indicates that the vegetation change reflects an upward trend. Conversely, if the slope is less than 0, it suggests a downward trend in vegetation change. Median" refers to the median value of these slopes.

Autocorrelation and Correlation analysis

To explore the spatial autocorrelation of NDVI data, we used the "global and local autocorrelation analysis based on Moran's I statistics." This method enables the evaluation of the average spatial differences between individual cells and their adjacent neighbors, thereby characterizing the spatial attributes of a specific property across the entire study area through global spatial autocorrelation analysis. In Moran's statistics, the normalized z-score can range from -1 to +1. A Moran's I value exceeding 0 indicates a positive correlation, which suggests a clustering pattern, while a value below 0 points to a negative correlation, reflecting a dispersed arrangement. The calculation of Moran's I statistics for examining spatial autocorrelation is provided by Xu et al. (2015):

$$I = \frac{N \sum_{i=1}^{n} \sum_{j=1}^{n} w_{ij} (x_i - \bar{x}) (x_j - \bar{x})}{\sum_{i=1}^{n} \sum_{j=1}^{n} w_{ij} \times \sum_{i=1}^{n} (x_i - \bar{x})^2}$$
(5)

Where N represents the number of observations, x_i denotes the observed value for cell i, x_j indicates the observed value for cell j, \bar{x} is the average of cell i or cell j, and w_{ij} is the weight assigned to the relationship between cells i and j.

While the global spatial autocorrelation through Moran's I statistics reveals the overall clustering pattern, it does not allow for the assessment of spatial association patterns across multiple locations. In contrast, Local Spatial Autocorrelation focuses on the significance of local statistics at each individual location and identifies the presence of spatial clusters, a capability that global spatial autocorrelation lacks. The mathematical equation of local spatial autocorrelation using Moran's I is described by (Anselin (2010)).

$$I_i = x_i \sum_{i=1, i \neq i}^N w_{ij} x_i \tag{6}$$

Relative weight analysis

Relative weight analysis (RWA) is a statistical technique commonly used in multiple regression analysis to assess the relative importance of predictor variables. It provides a way to estimate the proportional contribution of each predictor variable to the coefficient of determination (R-squared) while considering both their individual impact and their interactions with other variables (Johnson, 2020; Tonidandel et al., 2015). In this study, the RWA technique was used to assess the relative contributions of explanatory factors influencing NDVI mangrove dynamics.

Multiple linear regression assessment

In order to conduct a pixel-wise multiple linear regression analysis to examine the overall effects of climate variables on fluctuations in NDVI, various statistical measures were used to assess the strength of the spatiotemporal linear association. These measures included the slope and the coefficient of determination (R²) obtained from the regression model. The multiple linear regression model can be represented by the following equation:

$$Y_t = \alpha + \beta_1 X_{1t} + \beta_2 X_{2t} + \dots + \beta_n X_{nt} + \varepsilon, t \in \{1, 2, 3, \dots N\}$$
 (7)

where Y_t represents the NDVI time series, α -is the regression intercept, β is the regression slope, ε is the residual of the fit, X_t are the independent variables and t denotes the study period.

Partial correlation

The bivariate correlation coefficients may not effectively represent the complex relationships among variables in multivariate correlation analysis, given that multiple factors can influence these relationships. Therefore, partial correlation coefficients were computed to assess the spatiotemporal strength and direction of the linear relationship between NDVI and each climate variable, while controlling for the effects of the other climate variables (i.e, sea level, PET, SM, SPI, LST, TN and TX). The strongest correlation is close to 1, while the weakest is below 0.5. Thus, the partial correlation can be calculated as follow (Cheng et al., 2017):

$$R_{xy,z} = \frac{R_{xy} - B_{xz} R_{xy}}{\sqrt{(1 - R_{xy})^2} \sqrt{(1 - R_{yx})^2}}$$
(8)

Where x, y, and z represent three distinct variables. $R_{xy,z}$ signifies the partial correlation between variables x and y while accounting for the influence of variable z. Similarly, R_{xy} denotes the linear correlation coefficient between x and y, with R_{xz} and R_{yz} conveying analogous interpretations.

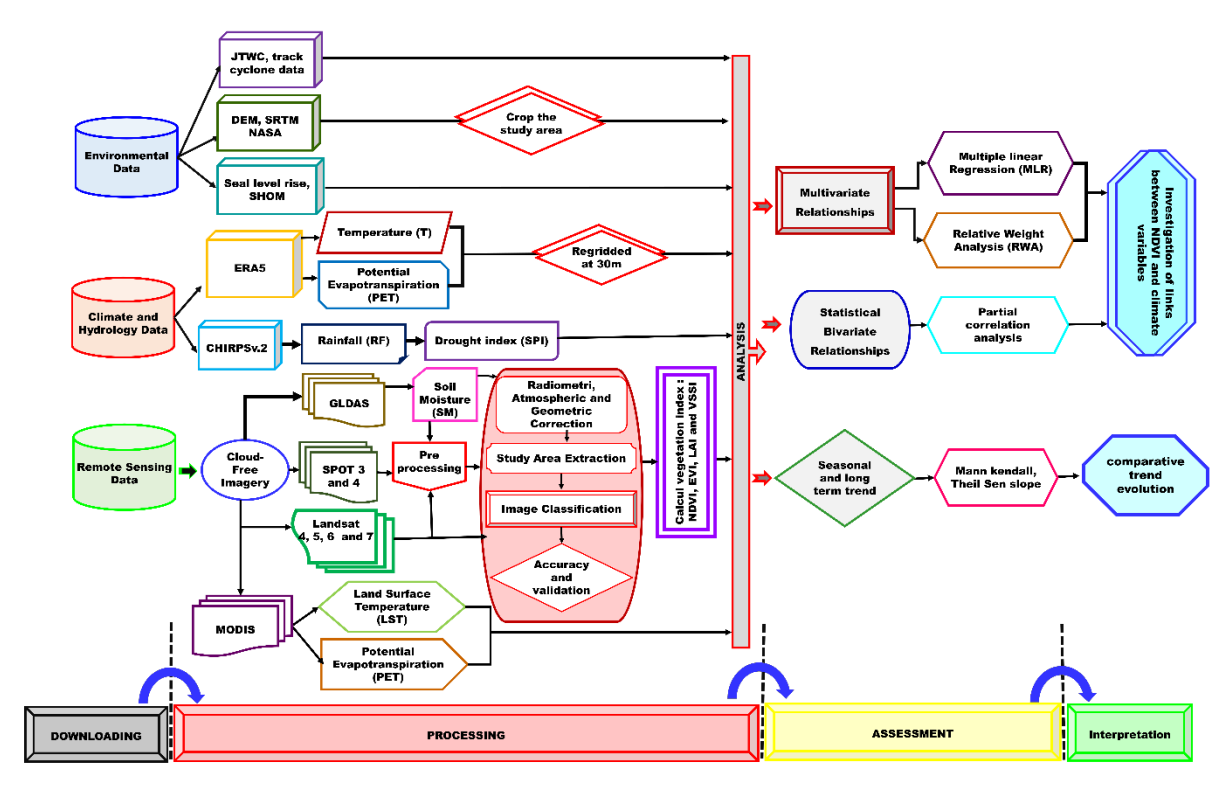


Fig. 2. Flowchart methodology of the study area.

Due to its extensive area of over 400 hectares, the mangrove forest at the Site was selected for this study to examine the relationship between NDVI and climatological and environmental parameters. NDVI is retained to study the relationships with these variables. Indeed, this index is useful for identification and has been employed in various applications (Li et al., 2019). Fig. 5 presents the interannual variability of various parameters, including NDVI, sea level (m), land surface temperature (LST) (°C), rainfall (mm), standardized precipitation index (SPI), minimum temperature (°C), maximum temperature (°C), soil moisture (mm), and potential evapotranspiration (PET) (mm) at the Site site from 1987 to 2022.

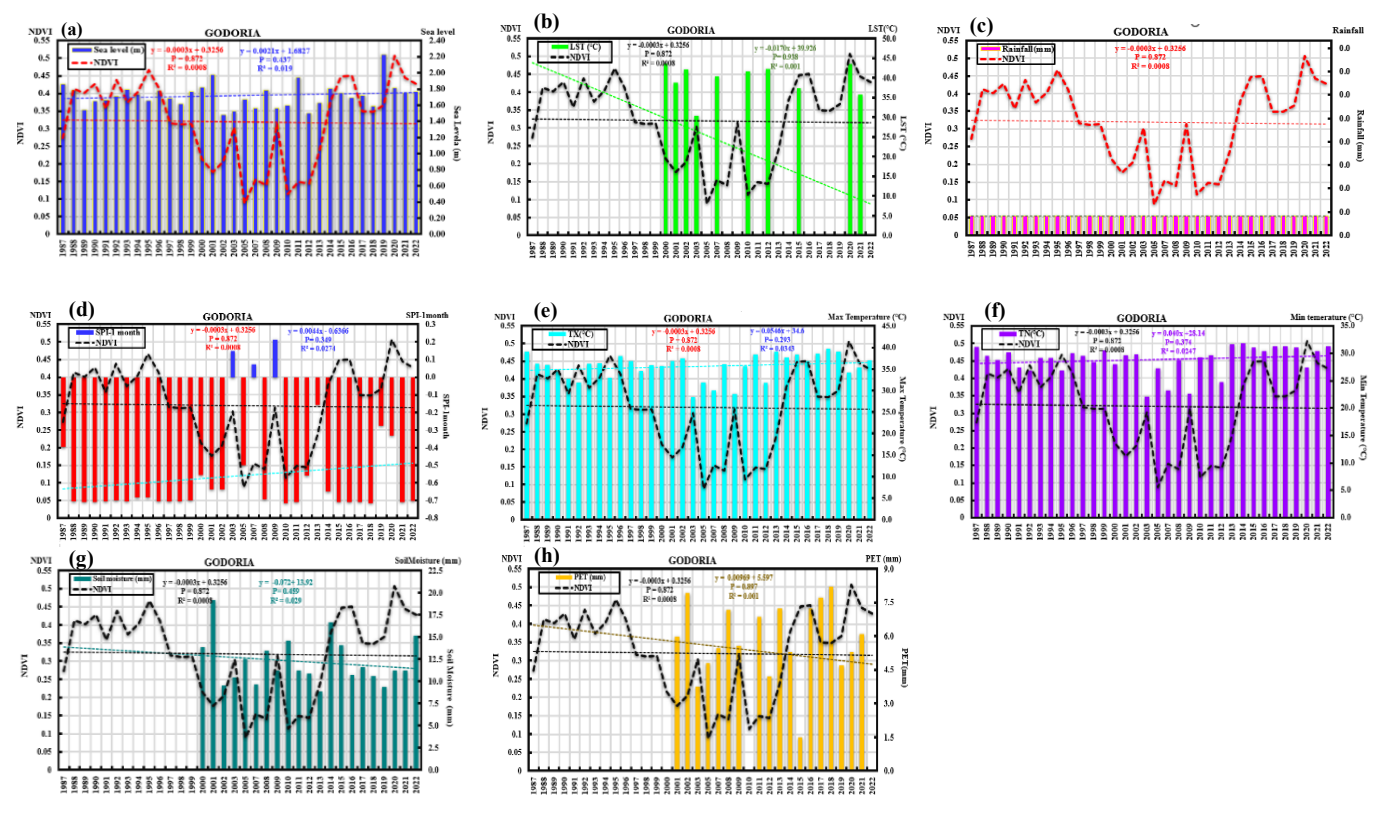


Fig. 5. Temporal variation of NDVI statistics and climate parameters from 1987 to 2022 at the Site, and - City mangrove site: (a) SL (m), LST (°C), (c) RF (mm), (d) SPI-1, (e) TN(°C), (f) TX (°C), (g) SM (mm) and (h) PET (mm).

Measuring spatial autocorrelations NDVI

In order to effectively assess the spatial dynamics of vegetation health, it is crucial to examine the local Normalized Difference Vegetation Index (NDVI) values within the context of their surrounding environments. Fig. 6 illustrates the distribution and clustering of NDVI values, revealing patterns of spatial autocorrelation and potential anomalies within the study area. The scatterplot Fig. 6a shows the dispersion of local NDVI values compared to the average NDVI of neighboring areas, based on a spatial weighting matrix. The points are grouped into four main quadrants: the High-High quadrant represents zones with high NDVI surrounded by high-value neighbors, indicating strong positive spatial autocorrelation, often associated with healthy vegetation. The Low-High quadrant reflects areas with low NDVI surrounded by high-value neighbors, suggesting spatial anomalies or outliers. In contrast, the High-Low quadrant shows areas of high NDVI surrounded by neighbors with low values, another form of spatial anomaly. The Low-Low quadrant highlights areas where both local NDVI and neighboring values are low, typically indicating degraded zones or low vegetation cover. A key transition occurs around 0.4, marking a threshold between favorable conditions and more degraded areas Fig. 6b. The local Moran's I index, ranging from -0.91 to +4.2. Negative values signify spatial dissimilarity, often indicating abrupt changes in vegetation, while positive values represent strong spatial clustering of similar NDVI values. Fig. 6c identifies spatial clusters, with High-High clusters indicating dense vegetation areas, mainly in the southern region, and Low-Low clusters indicating degraded areas, especially the north and south extremes. High-Low and Low-High clusters reveal spatial anomalies where significant contrasts exist between neighboring areas.

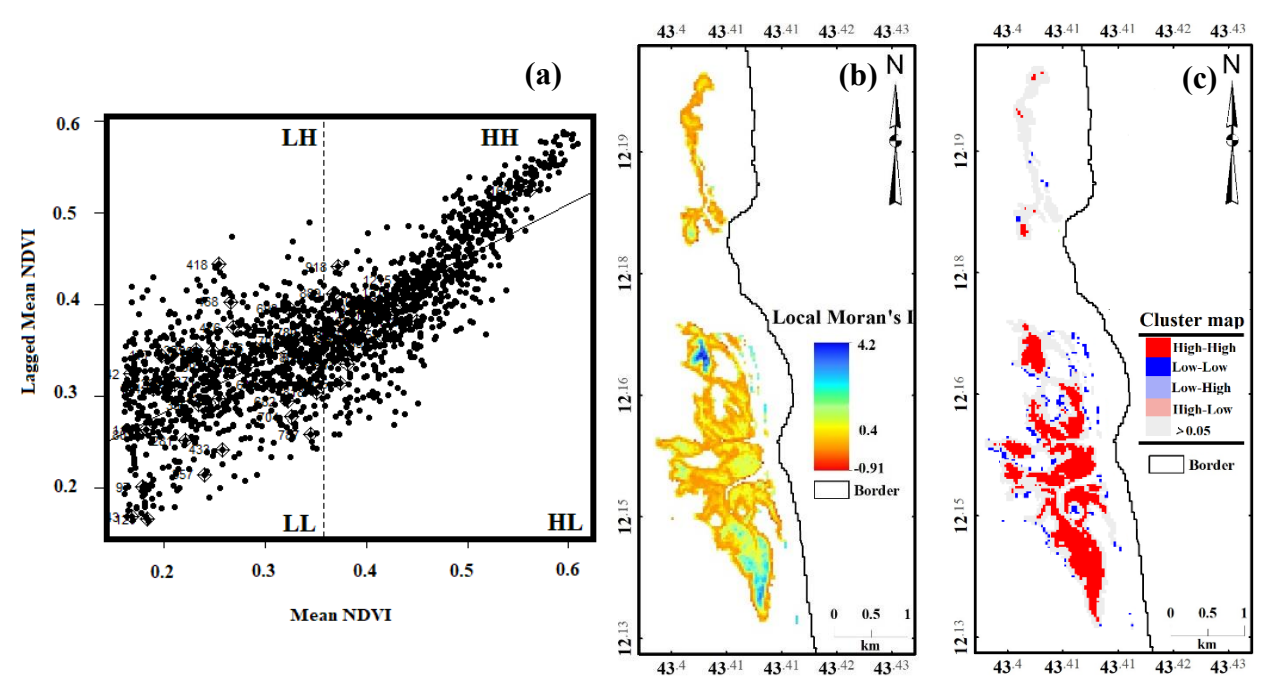


Fig. 6. Scatterplot of Local Moran's I and Spatial Autocorrelation of NDVI (a, b), and Cluster Map of Autocorrelation.

Geospatial distribution of NDVI and climate environmental variables

Fig. 7 presents the average values of NDVI and several hydroclimatic variables, including precipitation, potential evapotranspiration, soil moisture, minimum and maximum air temperatures, land surface temperature, and the digital elevation model, at the Site mangrove site for the period from 1987 to 2022. To ensure a consistent comparison, the climatic data were resampled to a resolution of 30 meters, aligning with that of the NDVI. From 1987 to 2022, the NDVI values at Site ranged from -0.07, indicating water bodies, to 0.45, representing moderate vegetation (Fig. 7a). The SPI-1 index exhibited values between -0.59 and -0.51, suggesting drought conditions that were more pronounced in the northern region of the Site mangrove (Fig. 7b). During the JJAS season (June to September), no precipitation was recorded due to the dry season and limited cloud cover, resulting in rainless days throughout this period (Fig. 7c). The potential evapotranspiration (PET) values varied from 0 to 213.97 mm, with higher levels observed in the southern part of Site compared to the north (Fig. 7d). Soil moisture (SM) ranged from 9.51 mm to 13.77 mm, showing lower values in the northern region than in the south (Fig. 7e). The minimum and maximum air temperatures were recorded at 28.74°C to 28.98°C and 34.93°C to 35.89°C, respectively, with slightly lower temperatures noted in northern Site compared to the south (Fig.

7f and Fig. 7g). The land surface temperature (LST) varied from 34.14°C to 42.38°C, with coastal mangroves generally cooler than those further inland (Fig. 7h). Elevation also appears to influence salinity levels related to sea level; higher terrain is primarily located in the central region of the Site mangrove. Additionally, according to the NASA SRTM DEM, the southern part of Site is situated on higher terrain compared to the northern area, with elevations ranging from 10 to 17 meters above sea level (Fig. 7i). This finding summarizes the climatic conditions in the Site region, providing a clearer understanding of the area's environmental context.

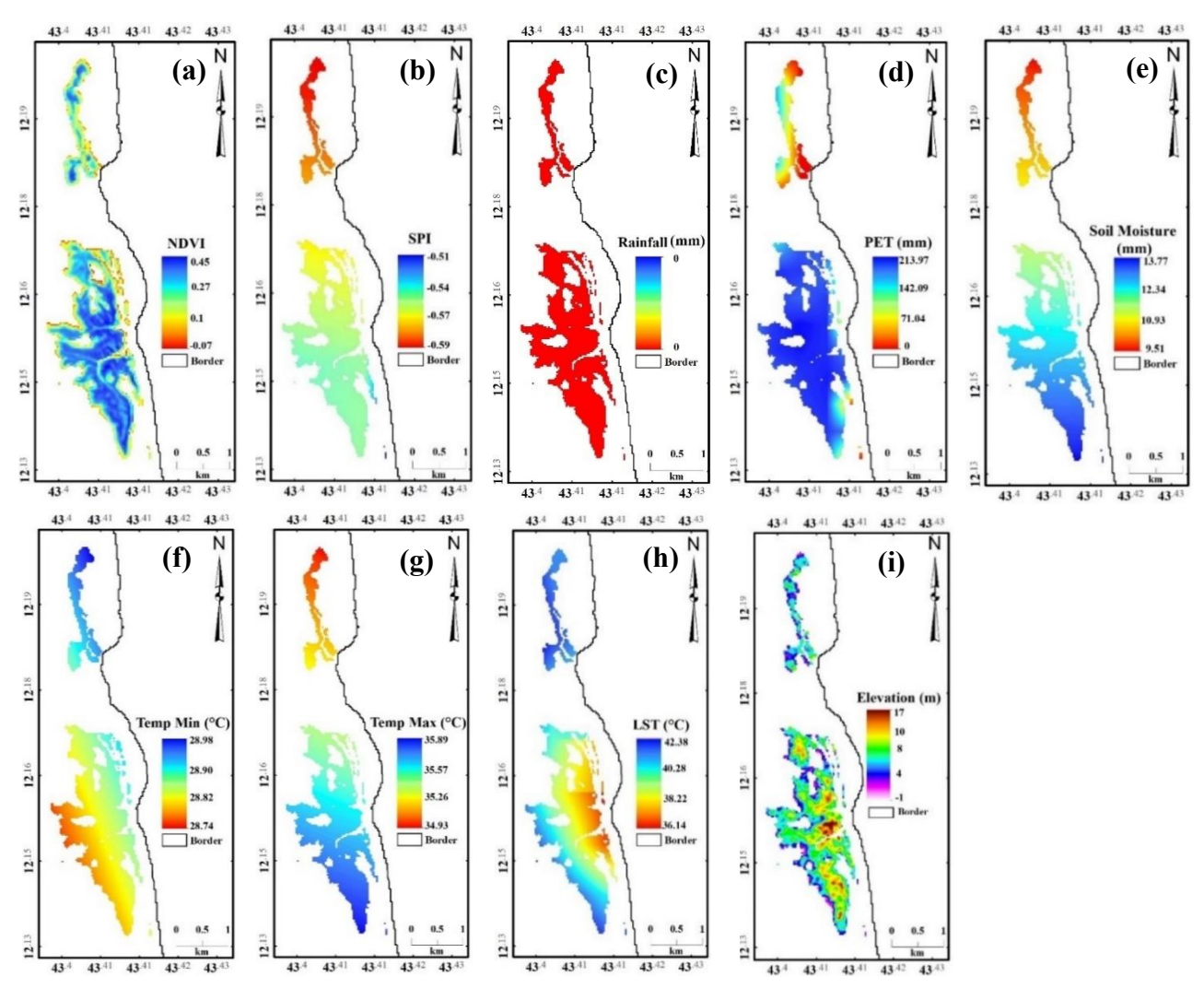
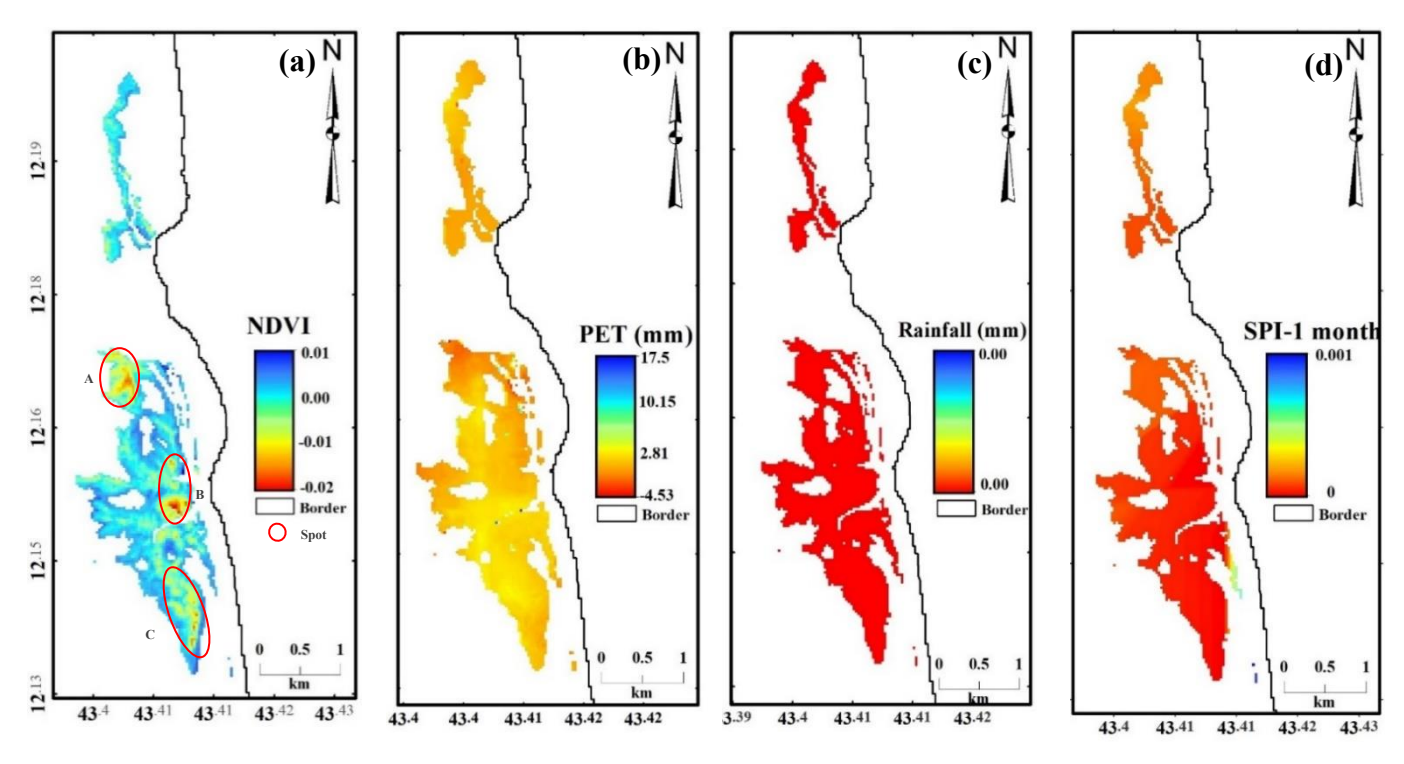


Fig. 7. Mean spatial distribution of NDVI (a), SPI-1 (b), RF (c), PET (d), SM (e), TN (f), TX (g), LST(h) and Digital Elevation model (DEM) (i) in Site mangrove area from 1987 to 2022.

Spatiotemporal patterns of trends evolution

Over the past 36 years, the NDVI has shown a decreasing trend in several localities in southern Site (Fig. 8a), with a decline rate ranging from -0.02 to 0.01 per year. However, an increasing trend is observed primarily at the extremities of southern Site, while the northern part of Site remains relatively stable overall. Alongside NDVI trends, Potential Evapotranspiration exhibits a general upward trend across the Site mangrove area (Fig. 8b). Both Rainfall and the Standardized Precipitation Index (SPI-1) remain largely neutral patterns with no significant trend (Figs. 8c and 8d). Meanwhile, soil moisture displays a negative trend, mainly in the Site area, ranging from -0.038 to -0.014 per year (Fig. 8e). The decrease in soil moisture levels can have significant implications for mangrove ecosystems, suggesting an increasing water deficit that may hinder the growth of mangrove species and reduce the overall resilience and productivity of these coastal habitats. In terms of temperature trends, both the minimum and maximum air temperatures show an increasing trend, with minimum temperatures rising between 0.049°C and 0.061°C and maximum temperatures increasing between 0.06°C and 0.08°C, respectively, from 1987 to 2022 (Fig. 8f, (Fig. 8g). Spatially, most of the increasing trends occurred in the northern part of Site compared to the south. At the same time, LST (Land Surface Temperature) shows an upward trend in the southeastern part of Site and, conversely, in the northern area (Fig. 8h). The rate of LST ranges from -0.47 to 0.023 per year. Our results indicate that, over the study period from 1987 to 2022, spatial trend variations in the Site mangrove area are more homogeneous for PET, rainfall, and, to a lesser extent, SPI-1 month and soil moisture. In contrast, minimum and maximum temperatures, along with LST, are generally higher in the southern region compared to the northern region.



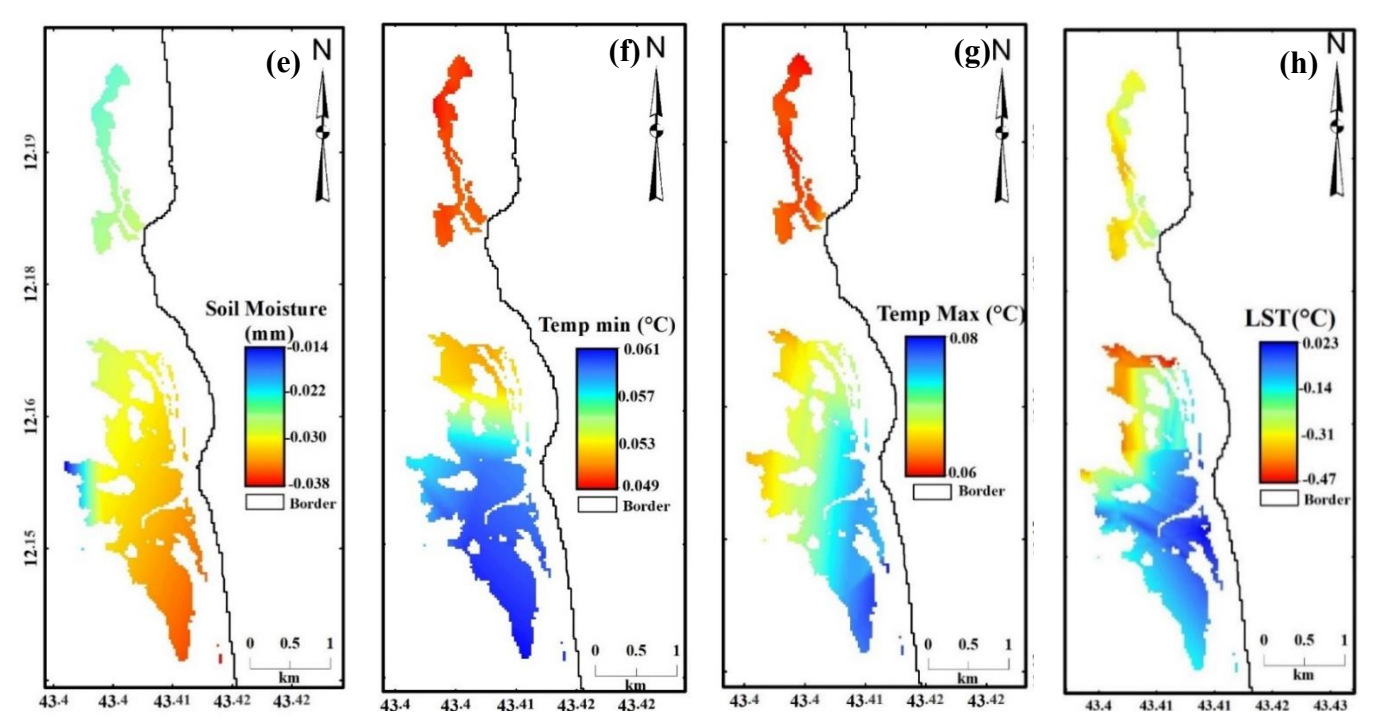


Fig. 8. The geospatial distributions of trends analyses for NDVI (a) and climate variables, including (b) PET (°C), (c) Rainfall (mm), (d) SPI, (e) Soil Moisture (mm), (f) Minimum Temperature (°C), (g) Maximum Temperature (°C), and (h) LST (°C), over the Site mangrove from 1987 to 2022.

Spatiotemporal of NDVI and climatic variables relationship analysis

Multi-temporal relation analysis

To better understand the relative importance of predictive variables in regression models, we employed a recent approach that evaluates how each variable contributes to the explained variance within the model using Relative Weights Analysis (RWA), focusing on the period from 1987 to 2022 for the Site site. The results indicate that sea level exhibits the most significant contribution, with a raw relative weight of 0.335, followed by soil moisture and maximum (TX) and minimum (TN) temperatures, which have raw relative weights of 0.080 and 0.081, respectively (Fig. 9a and Table S5). Notably, soil moisture and minimum temperature have negative influences, while sea level, maximum temperature, and minimum temperature show positive relationships (Fig. 9a). The land surface temperature (LST) and the one-month Standardized Precipitation Index (SPI-1month) also possess lower relative weights, indicating they have less impact on the observed variations. Furthermore, although the dry and hot season (JJAS) is characterized by a lack of precipitation, it was still represented in the analysis using the one-month Standardized Precipitation Index (SPI-1), which serves as a proxy indicator for drought conditions during this period. Additionally, Pearson correlation analysis reveals a moderate positive relationship between sea level and minimum temperature (TN), with a coefficient close to 0.4 (Fig. 9b). Conversely, the relationship between Potential Evapotranspiration (PET) and the considered variables is negative, with a coefficient of -0.33, suggesting that increased PET may be linked to a decrease in certain other climatic variables (Fig. 9b). Besides, the dry and hot season (JJAS) is characterized by minimal precipitation; thus, we use the one-month SPI index, which shows a negative correlation with mangrove NDVI. This negative correlation may suggest that an increase in soil moisture during this period corresponds with conditions less favorable for mangrove growth, possibly due to excess moisture levels. This result demonstrates that sea level, minimum and maximum temperatures, and PET are the most influential factors driving mangrove dynamics as reflected in NDVI variations. During drought periods, SPI, soil moisture, and LST have the least impact on NDVI fluctuations in the Site mangrove area over the study period from 1987 to 2022. Our findings align with the results of Akhter et al., 2024 and Hussien, et al., 2022. Furthermore, the dry and hot season (JJAS) is characterized by a lack of precipitation. This season was excluded from this analysis as its values do not vary significantly.

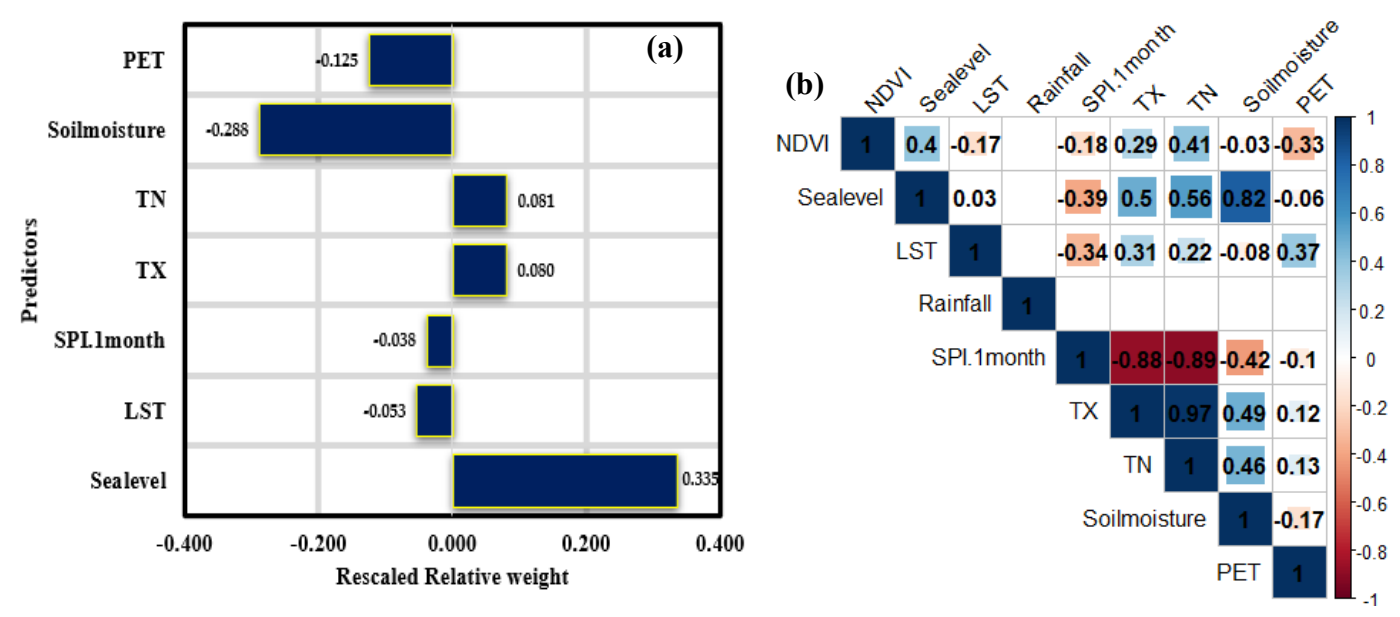
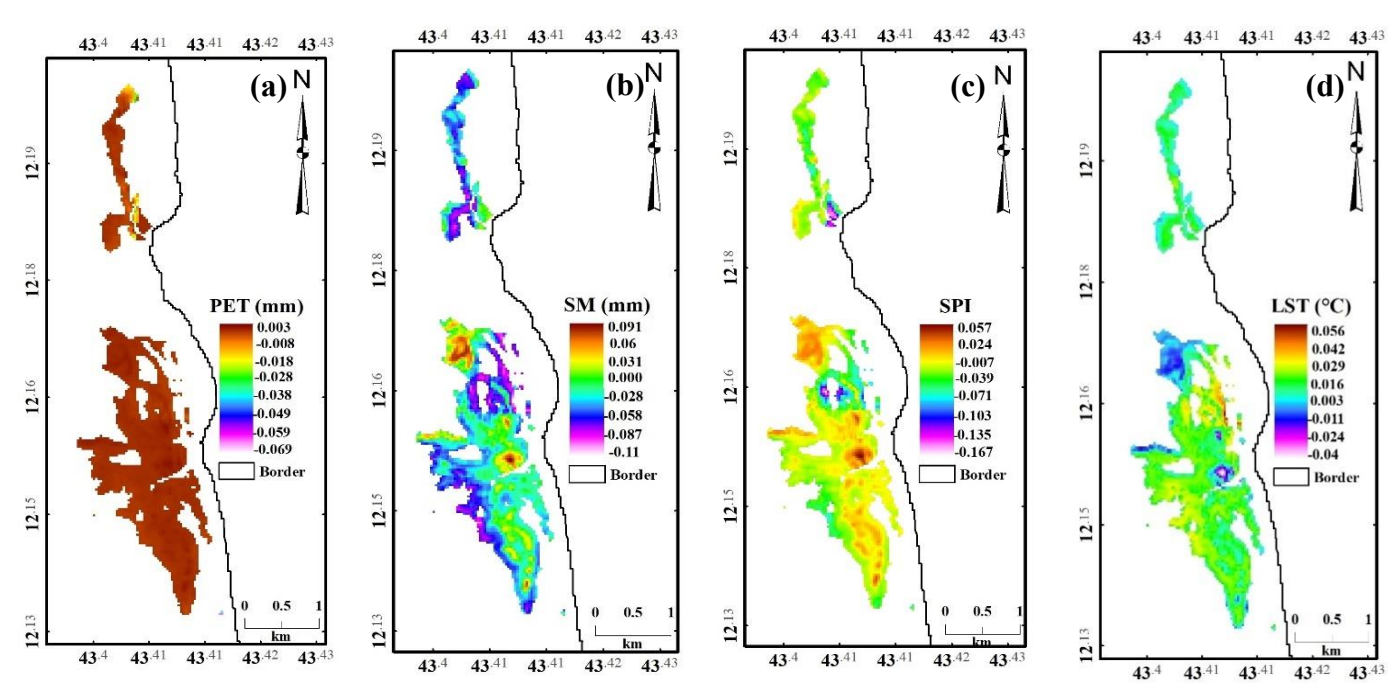


Fig. 9. (a)Estimation of relative importance of climate variables as predictors of NDVI. (b) Pearson correlation coefficient between NDVI and climate variables.

NDVI–Climate variables relationship's geographic patterns

To examine the relationship between NDVI and climatic variables in the context of geospatial variability, we applied multiple linear regression analysis. The slope coefficients (beta coefficients) indicate the strength and nature of these relationships. It can be observed that the beta coefficient for Potential Evapotranspiration (PET) is approximately zero over a significant portion of the study area, indicating negligible influence on NDVI. However, in certain small areas in the northern region, the coefficient is negative, indicating that increased PET leads to a decrease in NDVI (Fig. 10a). Over the last three decades, the relationship between soil moisture (SM) and NDVI is predominantly characterized by beta coefficients ranging from -0.11 to 0.00 in areas where NDVI demonstrates signs of recovery, while it is positive in regions where NDVI has declined (Fig. 10b). Similarly, the Standardized Precipitation Index (SPI) is positive in areas where NDVI has decreased and negative in areas where NDVI has shown recovery (Fig. 10c). Land Surface Temperature (LST) demonstrates a negative beta coefficient in regions with declining NDVI and conversely (Fig. 10d). Furthermore, both minimum and maximum air temperatures show a negative relationship where NDVI is declining and a positive relationship where NDVI is recovering (Figs. 10e and 10f). It should be noted that the coefficient of determination (local R²) values indicates how well the regression model fits the observed data. The local R² values range from 0 to 1. High R² values reflect better model performance, while low values suggest poorer fitting. Thus, the distribution of R² reveals that southern Site exhibits better performance compared to northern Site, with R² values generally exceeding 0.7 (Fig. 10g).



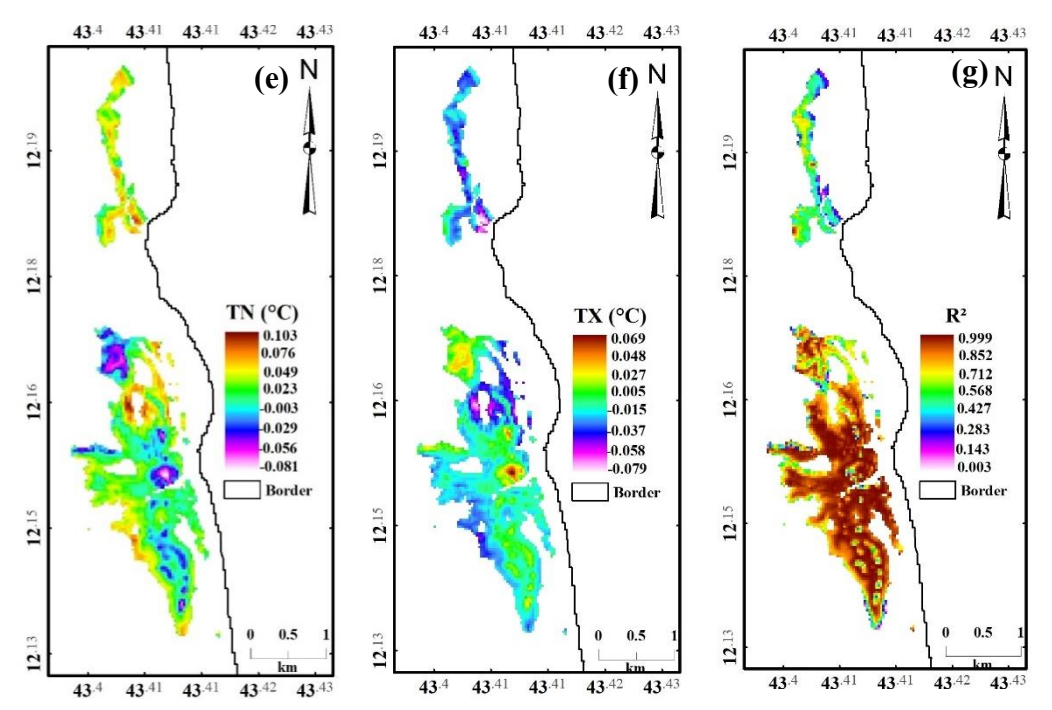


Fig. 10. The result of Multiple linear regression of NDVI and climate variable (PET, SM, SPI-1, LST, TN, and TX) over the Site mangrove from 1987 to 2022.

Table S6. Partial correlation between NDVI and climatic parameters.

	NDVI	SL	LST	RF	SPI.1	TX	TN	SM	PET
NDVI	1.000								
SL	-0.899	1.000							
LST	0.527	0.344	1.000						
SPI.1	0.767	0.411	-0.556	0.364	1.000				
TX	-0.759	-0.642	0.678	-0.291	0.580	1.000			
TN	0.874	0.685	-0.672	0.352	-0.774	0.952	1.000		
SM	0.002	0.030	-0.171	-0.011	0.067	0.169	-0.044	1.000	
PET	-0.746	-0.622	0.613	-0.294	0.632	-0.650	0.735	-0.101	1.000

On the other hand, the analysis of partial correlations between the NDVI of the Site mangrove and various climatic parameters from 1987 to 2022 reveals intriguing relationships (Table S6). The

NDVI, which indicates vegetation health, shows a strong negative partial correlation with sea level (PCC = -0.899), suggesting that rising sea levels could harm the health of the mangrove. This finding is consistent to those of Ruan et al. (2022). Besides, maximum temperature (TX) also exhibits a negative partial correlation with NDVI (PCC = -0.759), indicating that higher temperatures may be associated with vegetation degradation. In contrast, minimum temperature (TN) is positively correlated with NDVI (PCC = 0.874), suggesting that higher nighttime temperatures may promote mangrove growth. The positive partial correlation between NDVI and the SPI.1 index (PCC = 0.767) indicates that favorable wet conditions are beneficial for vegetation. The observed negative relationship between NDVI and precipitation (PCC = -2.558) could reflect a complex dynamic, such as soil saturation, while soil moisture shows a very weak partial correlation (PCC = 0.002), indicating that other factors may influence the health of the mangrove (Table S6). Our results show strong alignment with findings from comparable studies (Hussien et al., 2022; Ruan et al., 2022). These findings underscore the importance of an integrated approach to analyze the interactions between climatic variables and NDVI, providing insights into the potential impacts of climate change on this fragile ecosystem.

Conclusion

This study presents, for the first time, a long-term dataset of NDVI combined with innovative geospatial techniques to analyze changes in three distinct areas of mangrove ecosystems across spatial and temporal dimensions. This study compared the NDVI, EVI, and SAVI across the three study areas from 1987 to 2022, revealing a spatial reduction in bare soil and an increase in vegetation cover. However, a period of mangrove health degradation was noted between 2000 and 2012 across all three sites (i.e. Site, Island and City). The VSSI exhibited significant improvement along the Site region while remaining stable in the surrounding areas, particularly on Island, and City. The observed period of degradation may be attributed to various adverse climatic conditions, including an increase in SM, SPI, and decrease in TX, TN and PET. On the other hand, data from the JTWC indicate no significant impact from cyclonic activity in these regions during the period from 1987 to 2022. Besides, WorldPop data suggests the presence of buildings near the three mangrove areas, indicating a possible anthropogenic impact on mangrove ecosystems. In terms of interannual variability from 1987 to 2022, the NDVI in Site exhibited a slight downward trend, coinciding with decreases in LST and SM, while showing increases in sea level, SPI, TX, TN, and PET. Further, Relative Weights Analysis and partial correlation analyses indicated that the most influential parameters affecting NDVI variability were sea level, PET, TN, and TX. Moreover, multiple linear regression analyses revealed a more complex relationship across spatial scales. Each variable demonstrated both positive and negative coefficients, varying with terrain elevation. Degraded areas were identified in higher-altitude regions, particularly in Site, where negative coefficients were associated with TN and LST, while the SPI and soil moisture exhibited positive coefficients. PET was more uniformly distributed across the study areas, since 2012, the health of the mangroves has remained positively stable.

Conflicts of Interest

The author declare no conflict of interest.

References

Abatzoglou, J. T., Dobrowski, S. Z., Parks, S. A., & Hegewisch, K. C. (2018). TerraClimate, a high-resolution global dataset of monthly climate and climatic water balance from 1958–2015. Scientific Data, 5, 170191. doi:10.1038/sdata.2017.191

Ahamed, T., Tian, L., Zhang, Y., & Ting, K. C. (2011). A review of remote sensing methods for biomass feedstock production. Biomass and Bioenergy, 35(7), 2455–2469. doi:10.1016/j.biombioe.2011.02.028

Akhter, J., & Afroz, R. (2024). Influence of climate variability and land cover dynamics on the spatio-temporal NDVI patterns in western hydrological regions of Bangladesh. Heliyon, 10(12), Article e32625. https://doi.org/10.1016/j.heliyon.2024.e32625

Anselin, L. (2010). Lagrange Multiplier Test Diagnostics for Spatial Dependence and Spatial Heterogeneity. Geographical Analysis, 20(1), 1–17. doi:10.1111/j.1538-4632.1988.tb00159.x 4

Anu, K., Parveen, H., Sneha, V. K., Busheera, P., Muhammed, J., & Augustine, A. (2024). Mangroves in environmental engineering: Harnessing the multifunctional potential of nature's coastal architects for sustainable ecosystem management. Results in Engineering, 21, 101765. https://doi.org/10.1016/j.rineng.2024.101765.

Arceo-Carranza, D., Chiappa-Carrara, X., Chávez López, R., Yáñez Arenas, C. (2021). Mangroves as Feeding and Breeding Grounds. In: Rastogi, R.P., Phulwaria, M., Gupta, D.K. (eds) Mangroves: Ecology, Biodiversity and Management. Springer, Singapore. https://doi.org/10.1007/978-981-16-2494-0 3

Asari, N., Suratman, M.N., Mohd Ayob, N.A., Abdul Hamid, N.H. (2021). Mangrove as a Natural Barrier to Environmental Risks and Coastal Protection. In: Rastogi, R.P., Phulwaria, M., Gupta, D.K. (eds) Mangroves: Ecology, Biodiversity and Management. Springer, Singapore. https://doi.org/10.1007/978-981-16-2494-0 13

Banerjee A., Kang S., Meadows M.E., Sajjad W.,Bahadur A., Moazzam M.F.U., Xia Z., Mango J.,Das B., Kirsten K.L. 2024. Evaluating the relative influence of climate and human activities on recent vegetation dynamics in West Bengal, India,Environmental Research,250, https://doi.org/10.1016/j.envres.2024.118450.

Bashir, B.; Cao, C.; Naeem, S.; Zamani Joharestani, M.; Bo, X.; Afzal, H.; Jamal, K.; Mumtaz, F. Spatio-Temporal Vegetation Dynamic and Persistence under Climatic and Anthropogenic Factors. Remote Sens. 2020, 12, 2612. https://doi.org/10.3390/rs12162612

Bi, H., Ma, J., Zheng, W., & Zeng, J. (2016). Comparison of soil moisture in GLDAS model simulations and in situ observations over the Tibetan Plateau. Journal of Geophysical Research: Atmospheres, 121(6), 2658–2678. doi:10.1002/2015jd024131

- Camberlin, P., Assowe Dabar, O., Pohl, B., Mohamed Waberi, M., Hoarau, K., & Planchon, O. (2024). Contribution of Western Arabian Sea Tropical Cyclones to Rainfall in the Horn of Africa and Southern Arabian Peninsula. Journal of Geophysical Research: Atmospheres, 129(17), e2024JD041109. https://doi.org/10.1029/2024JD041109
- Chang, J.; Liu, Q.; Wang, S.; Huang, C. Vegetation Dynamics and Their Influencing Factors in China from 1998 to 2019. Remote Sens. 2022, 14, 3390. https://doi.org/10.3390/rs14143390
- Cheng, C. X., Wang, Z. H., Xiao, P. Q., Xu, Z. X., Jiao, P., Dong, G. T., & Wei, G. J. (2017). Spatio-temporal dynamics of NDVI and its response to climate factors in the Heihe River Basin, China. IOP Conference Series: Earth and Environmental Science, 82, 012045. doi:10.1088/1755-1315/82/1/012045
- Chisola, M. N., & Kuráž, M. (2016). Patterns and Implications of Hydrologic Regime Change in Chongwe River, Zambia. Journal of Geography and Geology, 8(3), 1. doi:10.5539/jgg.v8n3p1
- Congedo, L., (2021). Semi-Automatic Classification Plugin: A Python tool for the download and processing of remote sensing images in QGIS. Journal of Open Source Software, 6(64), 3172, https://doi.org/10.21105/joss.03172
- Courtois, M., &Traizet, M. (1986). *The SPOT satellites: From SPOT 1 to SPOT 4. Geocarto International*, 1(3), 4–14. doi:10.1080/10106048609354050
- Dagnachew, M., Kebede, A., Moges, A., & Abebe, A. (2020). Effects of Climate Variability on Normalized Difference Vegetation Index (NDVI) in the Gojeb River Catchment, Omo-Gibe Basin, Ethiopia. Advances in Meteorology, 2020, 1–16. doi:10.1155/2020/8263246
- Deval, K., & Joshi, P. K. (2021). Vegetation type and land cover mapping in a semi-arid heterogeneous forested wetland of India: comparing image classification algorithms. Environment, Development and Sustainability. doi:10.1007/s10668-021-01596-6
- Dooley, C. A., Boo, G., Leasure, D.R. and Tatem, A.J. 2020. Gridded maps of building patterns throughout sub-Saharan Africa, version 1.1. University of Southampton: Southampton, UK. Source of building footprints "Ecopia Vector Maps Powered by Maxar Satellite Imagery" 2020. doi:10.5258/SOTON/WP00677
- Ezaidi S., Aydda A., Kabbachi B., Althuwaynee O. F., Ezaidi A., HaddouM. A., Idoumskine I., Thorpe J., Park H-J., Kim S-W. 2022.Multi-temporal Landsat-derived NDVI for vegetation cover degradation for the period 1984-2018 in part of the Arganeraie Biosphere Reserve (Morocco). Remote Sensing Applications: Society and Environment,27,https://doi.org/10.1016/j.rsase.2022.100800
- Felicien Nkomeje. Comparative Performance of Multi-Source Reference Data to Assess the Accuracy of Classified Remotely Sensed Imagery: Example of Landsat 8 OLI Across Kigali City-Rwanda 2015. International Journal of Engineering Works, 2017, 4 (1), pp.10-20. ffhal-01455461
- Funk, C., Peterson, P., Landsfeld, M., et al. (2015). The Climate Hazards InfraRed Precipitation with Station data (CHIRPS) A New Precipitation Climate Data Set for the Developing World. *Scientific Data*, 2, 150066. https://doi.org/10.1038/sdata.2015.66

- Feng Gao, Masek, J., Schwaller, M., & Hall, F. (2006). On the blending of the Landsat and MODIS surface reflectance: predicting daily Landsat surface reflectance. IEEE Transactions on Geoscience and Remote Sensing, 44(8), 2207–2218. doi:10.1109/tgrs.2006.872081
- Geiger, R. Klassifikation der klimatenachW. Köppen. Landolt-Börnstein- Zahlenwerte Und Funkt. Aust. Phys. Chem. Astron. Geophys. Technol. 1954, 3, 603-607
- Ghosh S, C. P. (2015). A Review of Threats and Vulnerabilities to Mangrove Habitats: With Special Emphasis on East Coast of India. Journal of Earth Science & Climatic Change, 06(04). doi:10.4172/2157-7617.1000270
- Golestani M., Ghahfarokhi Z.M., Esfandiarpour-Boroujeni I., Shirani H.. 2023. Evaluating the spatiotemporal variations of soil salinity in Sirjan Playa, Iran using Sentinel-2A and Landsat-8 OLI imagery, CATENA, 231, https://doi.org/10.1016/j.catena.2023.107375.
- Hatfield, J.L.; Prueger, J.H. Value of Using Different Vegetative Indices to Quantify Agricultural Crop Characteristics at Different Growth Stages under Varying Management Practices. Remote Sens. 2010, 2, 562-578. https://doi.org/10.3390/rs2020562
- Hersbach, H., et al. (2020). "The ERA5 global reanalysis." *Quarterly Journal of the Royal Meteorological Society*, 146(730), 1999-2049. https://doi.org/10.1002/qj.3803
- Huete, A. (1988). A soil-adjusted vegetation index (SAVI). Remote Sensing of Environment, 25(3), 295–309. doi:10.1016/0034-4257(88)90106-x
- Hussien K., Kebede A., Mekuriaw A., Beza S. A., Erena S. H. 2023. Spatiotemporal trends of NDVI and its response to climate variability in the Abbay River Basin, Ethiopia, 9, https://doi.org/10.1016/j.heliyon.2023.e14113
- Islam, M. A., Jimmy, A. N., Alam, M. S., & Khan, N. A. (2021). The use of multi-temporal Landsat normalized difference vegetation index (NDVI) data for assessing forest cover change of Lawarchara National Park. Environment, Development and Sustainability. doi:10.1007/s10668-021-01408-x
- Islam, M. R., Khan, M. N. I., Khan, M. Z., & Roy, B. (2021). A three decade assessment of forest cover changes in Nijhumdwip national park using remote sensing and GIS. Environmental Challenges, 4, 100162. doi:10.1016/j.envc.2021.100162
- Johnson, J. W. (2000). A Heuristic Method for Estimating the Relative Weight of Predictor Variables in Multiple Regression. Multivariate Behavioral Research, 35(1), 1–19. doi:10.1207/s15327906mbr3501_1
- Joint Typhoon Warning Center. (2022). *Tropical cyclone warning center*. Retrieved from https://www.metoc.navy.mil/jtwc/jtwc.html?north-indian-ocean
- Kamal, M., Phinn, S., & Johansen, K. (2016). Assessment of multi-resolution image data for mangrove leaf area index mapping. Remote Sensing of Environment, 176, 242–254. doi:10.1016/j.rse.2016.02.013
- Kassaye Hussien, Asfaw Kebede, Asnake Mekuriaw, Solomon Asfaw Beza, Sitotaw Haile Erena. (2023). Spatiotemporal trends of NDVI and its response to climate variability in the Abbay River Basin, Ethiopia. Heliyon, https://doi.org/10.1016/j.heliyon.2023.e14113.

- Kathiresan, K., & Bingham, B. L. (2001). Biology of mangroves and mangrove Ecosystems. Advances in Marine Biology, 81–251. doi:10.1016/s0065-2881(01)40003-4
- UNESCO. 2015. https://whc.unesco.org/fr/listesindicatives/5961/5961/>. (Accessed 18/05/2023).
- Lamchin, M., Lee, W.-K., Jeon, S. W., Wang, S. W., Lim, C.-H., Song, C., & Sung, M. (2019). Corrigendum to "Mann-Kendall Monotonic Trend Test and Correlation Analysis using Spatiotemporal Dataset: the case of Asia using vegetation greenness and climate factors" [MethodsX 5 (2018) 803–807]. MethodsX, 6, 1379–1383. https://doi.org/10.1016/j.mex.2019.05.030
- Li, W., El-Askary, H., Qurban, M. A., Li, J., ManiKandan, K. P., & Piechota, T. (2019). *Using multi-indices approach to quantify mangrove changes over the Western Arabian Gulf along Saudi Arabia coast. Ecological Indicators*, 102, 734–745. https://doi.org/10.1016/j.ecolind.2019.03.047
- Nse, O. U., Okolie, C. J., & Nse, V. O. (2020). DYNAMICS OF LAND COVER, LAND SURFACE TEMPERATURE AND NDVI IN UYO CAPITAL CITY, NIGERIA. Scientific African, e00599. doi:10.1016/j.sciaf.2020.e00599
- Nguyen, K.-A., Liou, Y.-A., Tran, H.-P., Hoang, P.-P., & Nguyen, T.-H. (2020). Soil salinity assessment by using near-infrared channel and Vegetation Soil Salinity Index derived from Landsat 8 OLI data: a case study in the Tra Vinh Province, Mekong Delta, Vietnam. Progress in Earth and Planetary Science, https://doi.org/10.1186/s40645-019-0311-0
- Pang, G., Wang, X., & Yang, M. (2017). Using the NDVI to identify variations in, and responses of, vegetation to climate change on the Tibetan Plateau from 1982 to 2012. Quaternary International, 444, 87–96. doi:10.1016/j.quaint.2016.08.038
- Reiners, P.; Sobrino, J.; Kuenzer, C. Satellite-Derived Land Surface Temperature Dynamics in the Context of Global Change—A Review. *Remote Sens.* **2023**, *15*, 1857. https://doi.org/10.3390/rs15071857
- R.L. Wilby, S.Mora, A.O. Abdallah, A.Ortiz (2010). Confronting climate variability and change in Djibouti through risk management. 0 Taylor & Francis Group, London, ISBN 978-0-415-60034-7
- Robert, E. M. R., Schmitz, N., Okello, J. A., Boeren, I., Beeckman, H., & Koedam, N. (2010). Mangrove growth rings: fact or fiction? Trees, 25(1), 49–58. doi:10.1007/s00468-010-0487-9
- Rodrigues, A., Marçal, A. R. S., & Cunha, M. (2013). Identification of potential land cover changes on a continental scale using NDVI time-series from SPOT VEGETATION. International Journal of Remote Sensing, 34(22), 8028–8050. doi:10.1080/01431161.2013.828184
- Ruan, L., Yan, M., Zhang, L., Fan, X., & Yang, H. (2022). Spatial-temporal NDVI pattern of global mangroves: A growing trend during 2000–2018. Science of The Total Environment, 844, Article 157075. https://doi.org/10.1016/j.scitotenv.2022.157075
- Sandilyan, S., & Kathiresan, K. (2012). Mangrove conservation: a global perspective. Biodiversity and Conservation, 21(14), 3523–3542. doi:10.1007/s10531-012-0388-x
- Service hydrographique et océanographique de la marine (SHOM). (2022). Observations des données maritimes. https://maree.shom.fr

- Tsalyuk, M., Kelly, M., & Getz, W. M. (2017). Improving the prediction of African savanna vegetation variables using time series of MODIS products. ISPRS Journal of Photogrammetry and Remote Sensing, 131, 77–91. doi:10.1016/j.isprsjprs.2017.07.012 10.1016/j.isprsjprs.2017.07.012
- Tonidandel, S., LeBreton, J.M. RWA Web: A Free, Comprehensive, Web-Based, and User-Friendly Tool for Relative Weight Analyses. J Bus Psychol 30, 207–216 (2015). https://doi.org/10.1007/s10869-014-9351-z
- Wang, G., Wang, P., Wang, T.-Y., Zhang, Y.-C., Yu, J.-J., Ma, N., Frolova, N. L., & Liu, C.-M. (2019). Contrasting changes in vegetation growth due to different climate forcings over the last three decades in the Selenga-Baikal Basin. Remote Sensing, 11(4), 426. https://doi.org/10.3390/rs11040426
- Wang, J.; Fan, Y.; Yang, Y.; Zhang, L.; Zhang, Y.; Li, S.; Wei, Y. Spatial-Temporal Evolution Characteristics and Driving Force Analysis of NDVI in the Minjiang River Basin, China, from 2001 to 2020. Water 2022, 14, 2923. https://doi.org/10.3390/w14182923
- Witsen, D. B. (2012). Mangrove restoration and management in Djibouti: Criteria and conditions for success. Virginia Polytechnic Institute and State University.https://pdf.usaid.gov/pdf docs/pnaed179.pdf
- Wu, S.-T., & Chen, Y.-S. (2016). Examining eco-environmental changes at major recreational sites in Kenting National Park in Taiwan by integrating SPOT satellite images and NDVI. Tourism Management, 57, 23–36. doi:10.1016/j.tourman.2016.05.006
- Xu, S., Wu, C., Wang, L., Gonsamo, A., Shen, Y., & Niu, Z. (2015). A new satellite-based monthly precipitation downscaling algorithm with non-stationary relationship between precipitation and land surface characteristics. Remote Sensing of Environment, 162, 119–140. doi:10.1016/j.rse.2015.02.024
- Young, N. E., Anderson, R. S., Chignell, S. M., Vorster, A. G., Lawrence, R., & Evangelista, P. H. (2017). A survival guide to Landsat preprocessing. Ecology, 98(4), 920–932. doi:10.1002/ecy.1730
- Zhang, H., Chang, J., Zhang, L. et al. NDVI dynamic changes and their relationship with meteorological factors and soil moisture. Environ Earth Sci 77, 582 (2018). https://doi.org/10.1007/s12665-018-7759-x
- Hickey, S. M., Radford, B., Callow, J. N., & et al. (2021). ENSO feedback drives variations in dieback at a marginal mangrove site. Scientific Reports, 11, 8130. https://doi.org/10.1038/s41598-021-87341-5
- Pastor-Guzman, J., Dash, J., & Atkinson, P. M. (2018). Remote sensing of mangrove forest phenology and its environmental drivers. Remote Sensing of Environment, 205, 71–84. doi:10.1016/j.rse.2017.11.009
- Galeano, A., Urrego, L. E., Botero, V., & Bernal, G. (2017). Mangrove resilience to climate extreme events in a Colombian Caribbean Island. Wetlands Ecology and Management, 25(6), 743–760. doi:10.1007/s11273-017-9548-9

- Songsom, V., Koedsin, W., Ritchie, R. J., & Huete, A. (2019). Mangrove Phenology and Environmental Drivers Derived from Remote Sensing in Southern Thailand. Remote Sensing, 11(8), 955. https://doi.org/10.3390/rs11080955
- Abhik, S., Hope, P., Hendon, H.H. et al. Influence of the 2015–2016 El Niño on the record-breaking mangrove dieback along northern Australia coast. Sci Rep 11, 20411 (2021). https://doi.org/10.1038/s41598-021-99313-w
- De Jong Cleyndert, G., Cuni-Sanchez, A., Seki, H. A., Shirima, D. D., Munishi, P. K. T., Burgess, N., ... Marchant, R. (2020). The effects of seaward distance on above and below ground carbon stocks in estuarine mangrove ecosystems. Carbon Balance and Management, 15(1). doi:10.1186/s13021-020-00161-4
- Amaral, C., Poulter, B., Lagomasino, D., Fatoyinbo, T., Taillie, P., Lizcano, G., Canty, S., Herrera Silveira, J. A., Teutli-Hernández, C., Cifuentes-Jara, M., Charles, S. P., Moreno, C. S., González-Trujillo, J. D., & Roman-Cuesta, R. M. (2023). Drivers of mangrove vulnerability and resilience to tropical cyclones in the North Atlantic Basin. Science of The Total Environment, 898, 165413. https://doi.org/10.1016/j.scitotenv.2023.165413
- Rohli, R. V., Ates, S. A., Rivera-Monroy, V. H., Polito, M. J., Midway, S. R., Castañeda-Moya, E., ... Makoto, S. (2019). Interannual Hydroclimatic Variability in Coastal Tanzania. International Journal of Climatology. doi:10.1002/joc.6103
- Alongi, D.M. (2022). Climate Change and Mangroves. In: Das, S.C., Pullaiah, Ashton, E.C. (eds) Mangroves: Biodiversity, Livelihoods and Conservation . Springer, Singapore. https://doi.org/10.1007/978-981-19-0519-3 8
- Ruan, L., Yan, M., Zhang, L., Fan, X., & Yang, H. (2022). Spatial-temporal NDVI pattern of global mangroves: A growing trend during 2000–2018. Science of The Total Environment, 844, 157075. https://doi.org/10.1016/j.scitotenv.2022.157075
- Kumar, A., Anju, T., Archa, V., Warrier, V. P., Kumar, S., Goud, G. S., Kashyap, A. K., Singh, S., Komal, & Singh, P. (2021). Mangrove Forests: Distribution, Species Diversity, Roles, Threats and Conservation Strategies. In S. Sharma, & P. Singh (Eds.), Wetlands Conservation: Current Challenges and Future Strategies (pp. 229-271). John Wiley & Sons Ltd. https://doi.org/10.1002/9781119692621.ch12
- Lombard, F., Soumaré, S., Andrieu, J., & Josselin, D. (2023). Mangrove zonation mapping in West Africa, at 10-m resolution, optimized for inter-annual monitoring. Ecological Informatics, 75, 102027. https://doi.org/10.1016/j.ecoinf.2023.102027
- Maina, J. M., Bosire, J. O., Kairo, J. G., Bandeira, S. O., Mangora, M. M., Macamo, C., Ralison, H., & Majambo, G. (2021). Identifying global and local drivers of change in mangrove cover and the implications for management. Global Ecology and Biogeography, 30(10), 2133–2147. https://doi.org/10.1111/geb.13368
- Alatorre, L. C., Sánchez-Carrillo, S., Miramontes-Beltrán, S., Medina, R. J., Torres-Olave, M. E., Bravo, L. C., Wiebe, L. C., Granados, A., Adams, D. K., Sánchez, E., & Uc, M. (2016). Temporal

changes of NDVI for qualitative environmental assessment of mangroves: Shrimp farming impact on the health decline of the arid mangroves in the Gulf of California (1990–2010). Journal of Arid Environments, 125, 98–109. https://doi.org/10.1016/j.jaridenv.2015.10.010

Ceesay, A., Dibi, N. H., Njie, E., Wolff, M., & Koné, T. (2017). Mangrove vegetation dynamics of the Tanbi Wetland National Park in The Gambia. Environment and Ecology Research, 5(2), 145–160. https://doi.org/10.13189/eer.2017.050209

Duncan, C., Owen, H. J. F., Thompson, J. R., Koldewey, H. J., Primavera, J. H., & Pettorelli, N. (2018). Satellite remote sensing to monitor mangrove forest resilience and resistance to sea level rise. Methods in Ecology and Evolution, 9(8), 1837–1847. https://doi.org/10.1111/2041-210X.12923

Almahasheer, H., Aljowair, A., Duarte, C. M., & Irigoien, X. (2016). Decadal stability of Red Sea mangroves. Estuarine, Coastal and Shelf Science, 169, 164–172. doi:10.1016/j.ecss.2015.11.027

Mallick, J.; AlMesfer, M.K.;Singh, V.P.; Falqi, I.I.; Singh, C.K.;Alsubih, M.; Kahla, N.B. Evaluating the NDVI–Rainfall Relationship in BishaWatershed, Saudi Arabia Using Non-Stationary Modeling Technique.

Atmosphere 2021, 12, 593. https://doi.org/10.3390/atmos12050593

Akhter, J., & Afroz, R. (2024). Influence of climate variability and land cover dynamics on the spatio-temporal NDVI patterns in western hydrological regions of Bangladesh. Heliyon, 10, e32625. https://doi.org/10.1016/j.heliyon.2024.e32625

Ellison, J. C., & Zouh, I. (2012). Vulnerability to Climate Change of Mangroves: Assessment from Cameroon, Central Africa. Biology, 1(3), 617-638. https://doi.org/10.3390/biology1030617

Boateng, I. (2018). An Assessment of Vulnerability and Adaptation of Coastal Mangroves of West Africa in the Face of Climate Change. Threats to Mangrove Forests, 141–154. doi:10.1007/978-3-319-73016-5 7

Ward, R. D., Friess, D. A., Day, R. H., & Mackenzie, R. A. (2016). Impacts of climate change on mangrove ecosystems: a region by region overview. Ecosystem Health and Sustainability, 2(4), e01211. doi:10.1002/ehs2.1211

Sinsin, C. B. L., Salako, K. V., Fandohan, A. B., Kouassi, K. E., Sinsin, B. A., & Glèlè Kakaï, R. (2021). Potential climate change induced modifications in mangrove ecosystems: a case study in Benin, West Africa. Environment, Development and Sustainability. doi:10.1007/s10668-021-01639-y

Apostolopoulos, D. N., & Nikolakopoulos, K. G. (2022). SPOT vs Landsat satellite images for the evolution of the north Peloponnese coastline, Greece. Regional Studies in Marine Science, 56, 102691. https://doi.org/10.1016/j.rsma.2022.102691

Harvey, K. R., & Hill, G. J. E. (2001). Vegetation mapping of a tropical freshwater swamp in the Northern Territory, Australia: A comparison of aerial photography, Landsat TM and SPOT satellite imagery. International Journal of Remote Sensing, 22(15), 2911–2925. doi:10.1080/01431160119174

Latifi, H., Fassnacht, F. E., & Dech, S. (2014). Object-based extraction of bark beetle (Ips typographus L.) infestations using multi-date LANDSAT and SPOT satellite imagery. Progress in Physical Geography: Earth and Environment, 38(6), article 0309133314550670. https://doi.org/10.1177/0309133314550670

Sewilam, H., Hassan, B. T., & Khalil, B. S. (2024). Spatiotemporal distribution of mangrove along the Egyptian Red Sea coast and analysis of hydrological impact on growth patterns. International Journal of Environmental Science and Technology. https://doi.org/10.1007/s13762-024-05670-0

Guo Y, Liao J, Shen G. Mapping Large-Scale Mangroves along the Maritime Silk Road from 1990 to 2015 Using a Novel Deep Learning Model and Landsat Data. Remote Sensing. 2021; 13(2):245. https://doi.org/10.3390/rs13020245

Mohamed, M.K.; Adam, E.; Jackson, C.M. The Spatial and Temporal Distribution of Mangrove Forest Cover from 1973 to 2020 in Chwaka Bay and Menai Bay, Zanzibar. Appl. Sci. 2023, 13, 7962. https://doi.org/10.3390/app13137962

Hamza AJ, Esteves LS, Cvitanović M. Changes in Mangrove Cover and Exposure to Coastal Hazards in Kenya. Land. 2022; 11(10):1714. https://doi.org/10.3390/land11101714

Supplementary Information

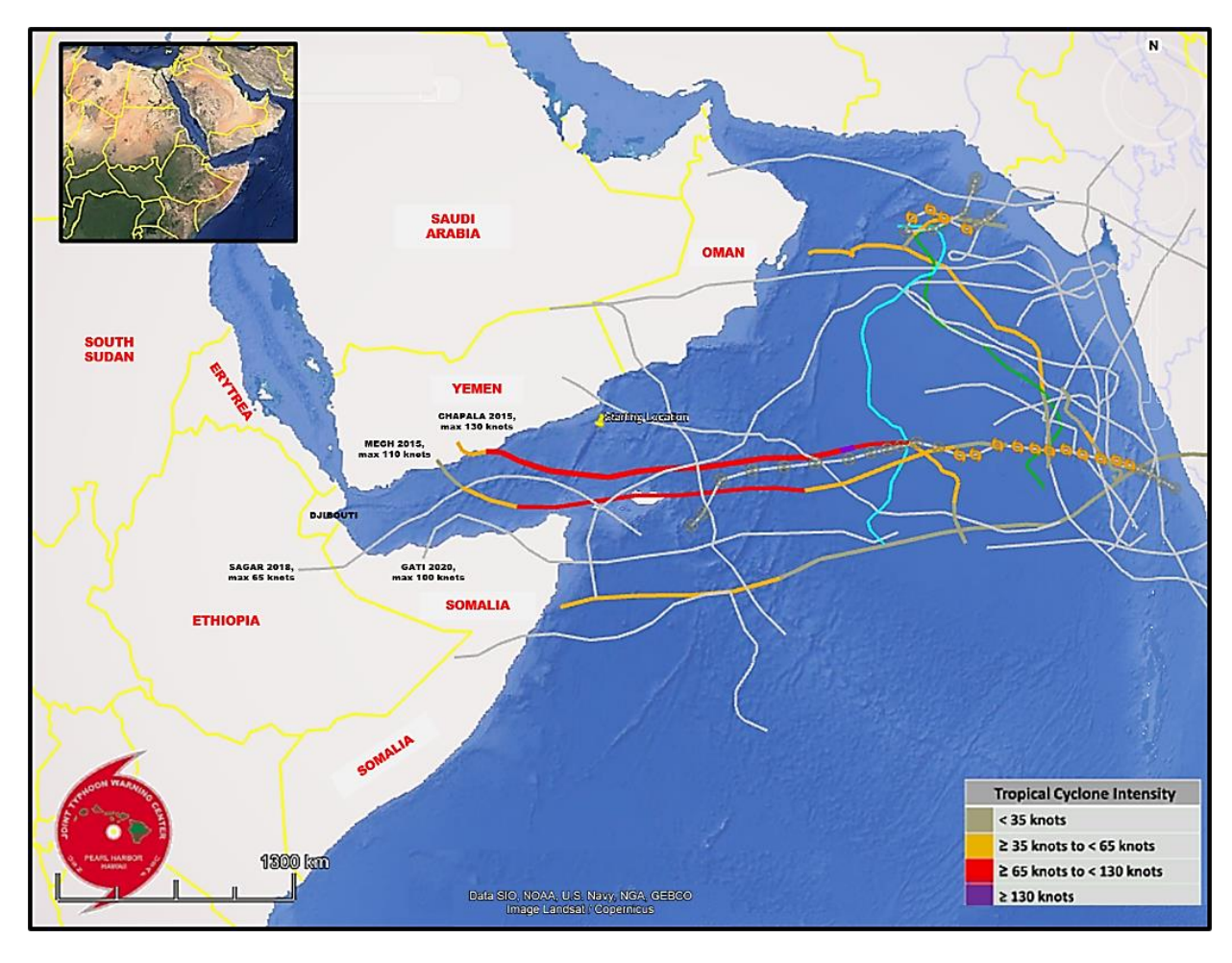
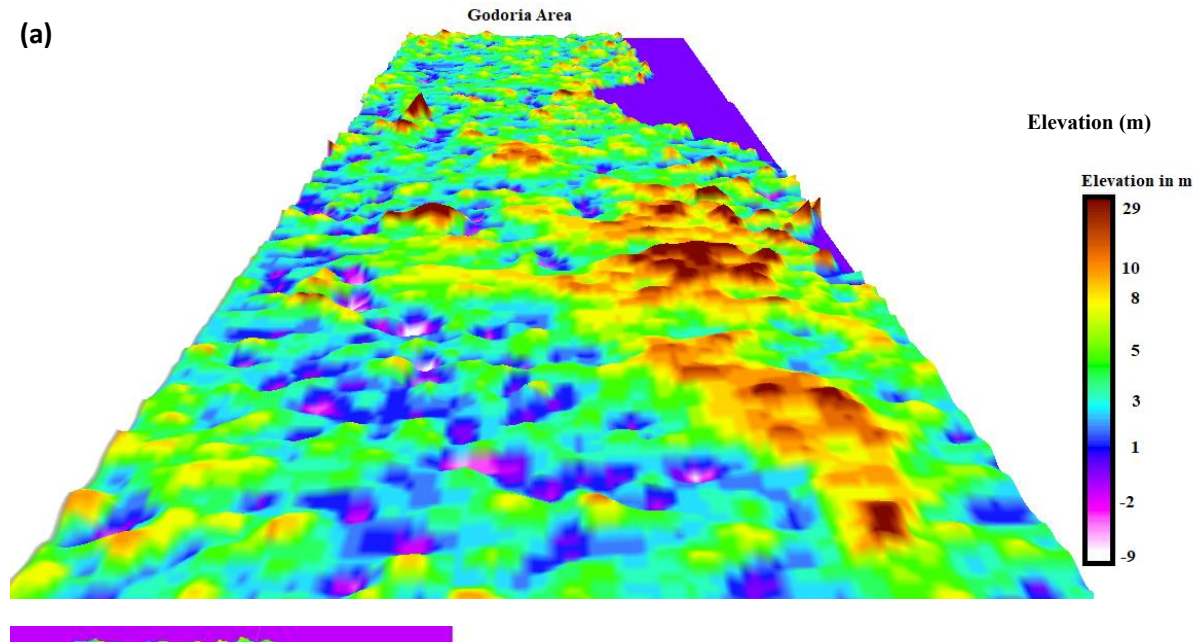
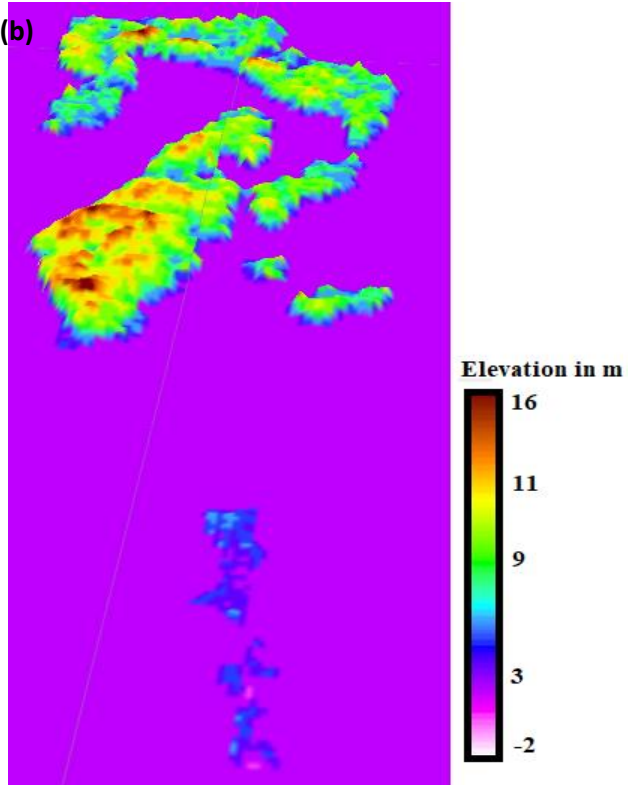


Fig. S7. Monitoring of Tropical Cyclones in the Horn of Africa by JTWC from 1980 to 2022.





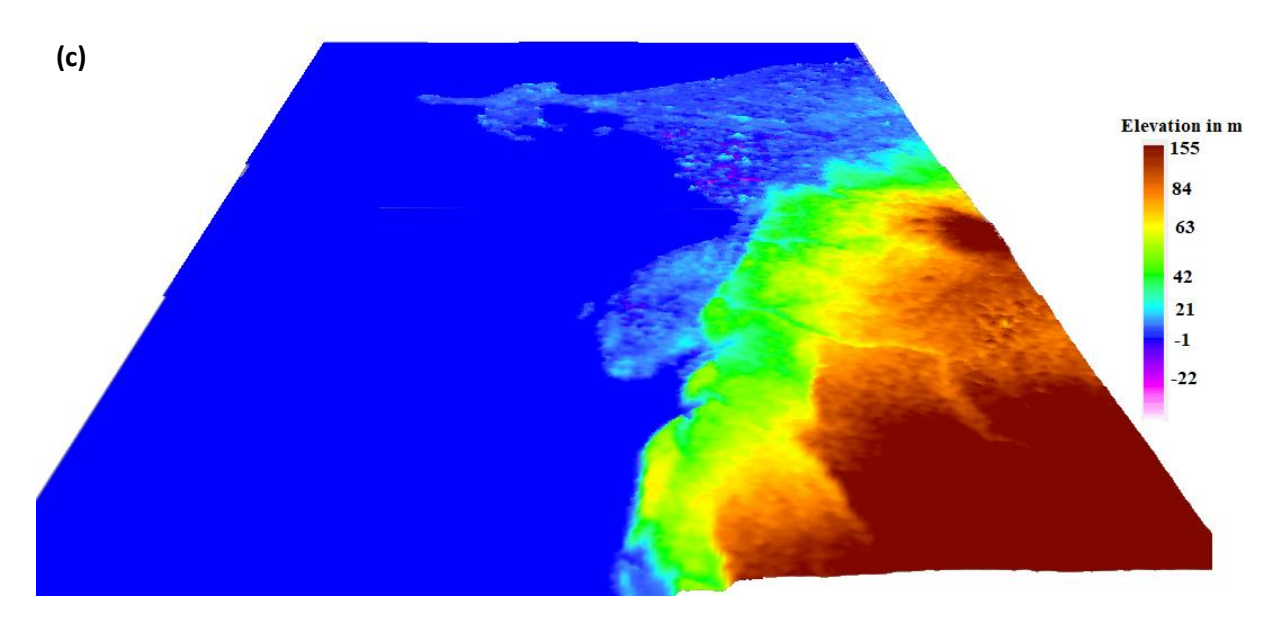


Fig. S8. 3D representation of SRTM NASA Digital Elevation Model Analysis of Mangrove Zones in (a), (b) Island, and (c) -City.

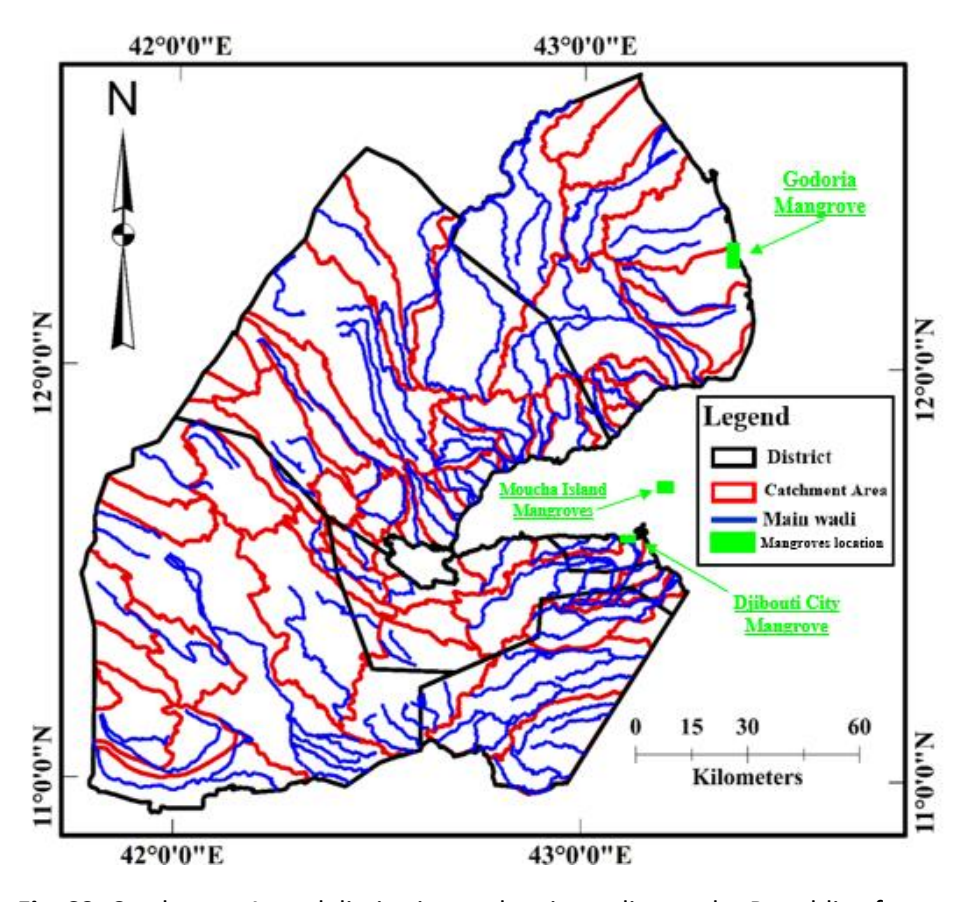


Fig. S9. Catchment Area delimitation and main wadi over the Republic of .

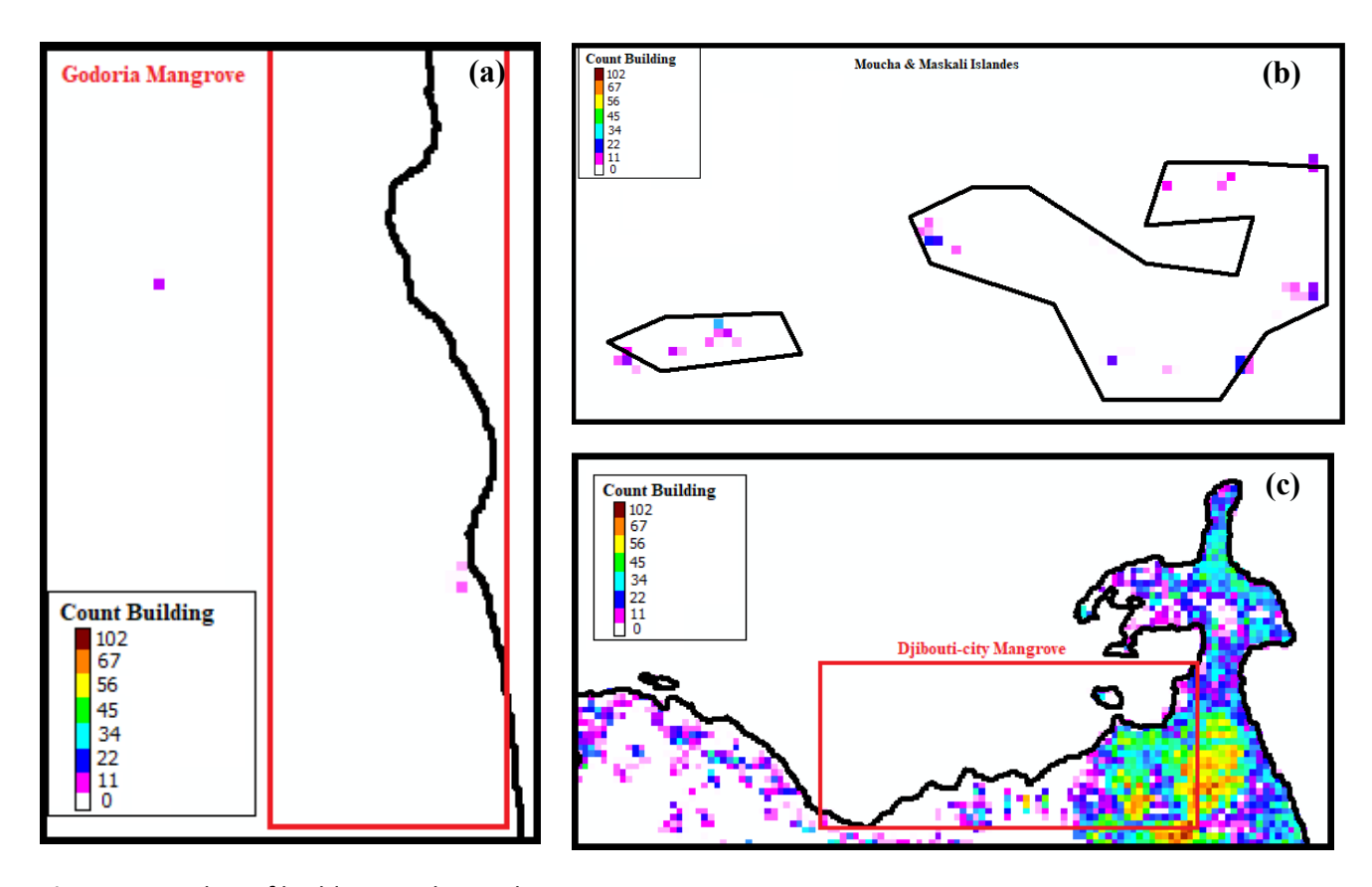


Fig. S10. Number of buildings in the study areas.

Table S4. Averaged grid of NDVI and climatic variables over Mangrove during the period 1987 to 2022.

	NA	MEAN	SD	MEDIAN	TRIM	MAD	MIN	MAX	RANGE	SKEW	KUR	SE
	(%)				MED						TOSIS	
NDVI	100	0.32	0.12	0.35	0.33	0.12	0.09	0.51	0.42	-0.45	-1.11	0.02
SL	100	1.72	0.15	1.71	1.71	0.12	1.48	2.23	0.75	1.05	2.02	0.03
LST	29	39.55	4.17	40.94	40.19	3.51	30.3	43.69	13.39	-0.95	-0.28	1.32
RF	100	0	0	0	0	0	0	0	0	NaN	NaN	0
SPI-1	100	-0.56	0.26	-0.7	-0.62	0.02	-0.72	0.21	0.93	1.8	2.02	0.05
TX	100	35.56	2.93	36.19	35.84	2.64	28.52	39.63	11.11	-0.77	-0.32	0.5
TN	100	28.85	2.54	29.54	29.21	2.21	22.1	31.86	9.76	-1.21	0.72	0.44
SM	62	12.2	2.61	11.22	11.89	2.26	8.86	19.16	10.3	0.98	0.24	0.57
PET	53	5.83	1.7	5.77	5.95	1.84	1.49	8.21	6.72	-0.67	0.03	0.4